JOURNAL OF THE AMERICAN CHEMICAL SOCIETY

Article

Dimer-of-Dimers Model for the Oxygen-Evolving Complex of Photosystem II. Synthesis and Properties of [MnO(terpy)(HO)](ClO)

Hongyu Chen, J. W. Faller, Robert H. Crabtree, and Gary W. Brudvig

J. Am. Chem. Soc., **2004**, 126 (23), 7345-7349• DOI: 10.1021/ja037389l • Publication Date (Web): 19 May 2004

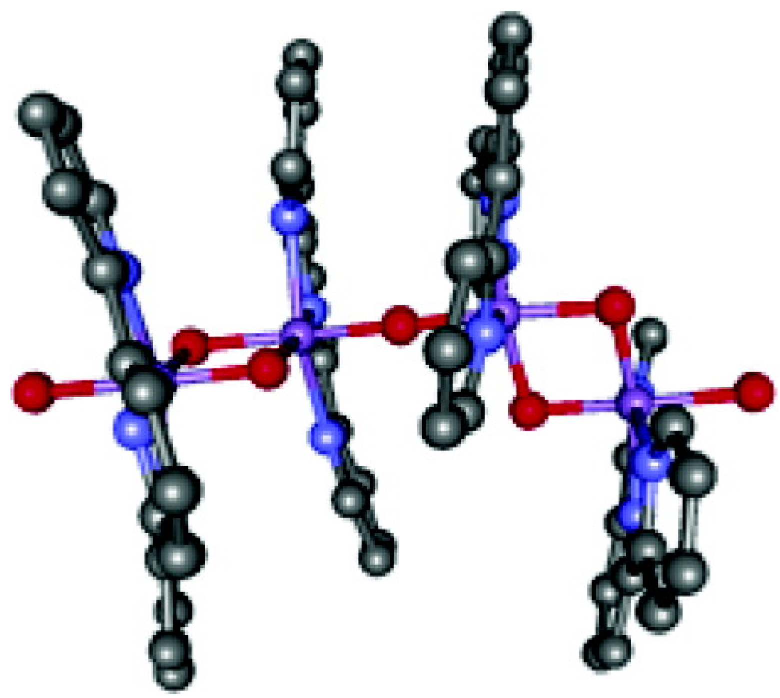

Journal of the American Chemical Society is published by the American Chemical Society. 1155 Sixteenth Street N.W., Washington, DC 20036

JACS ARTICLES

Published on Web 05/19/2004

Dimer-of-Dimers Model for the Oxygen-Evolving Complex of Photosystem II. Synthesis and Properties of $[Mn^{IV}_4O_5(terpy)_4(H_2O)_2](ClO_4)_6$

Hongyu Chen, J. W. Faller, Robert H. Crabtree,* and Gary W. Brudvig*

Contribution from the Department of Chemistry, Yale University, P.O. Box 208107, New Haven, Connecticut 06520-8107

Received July 18, 2003; E-mail: gary.brudvig@yale.edu; robert.crabtree@yale.edu

Abstract: A dimer-of-dimers model compound for the oxygen-evolving complex of photosystem II, $[\{(H_2O)(terpy)Mn^{IV}(\mu\text{-}O)_2Mn^{IV}(terpy)\}_2(\mu\text{-}O)](ClO_4)_6$ (terpy = 2,2′:6′,2″-terpyridine), has been prepared and characterized by X-ray crystallography and ESI-MS. Low pH was found to promote the disproportionation of $[Mn^{III/IV}{}_2O_2(terpy)_2(OH_2)_2]^{3+}$ to Mn^{2+} and a $Mn^{IV/IV}{}_2O_2(terpy)_2$ species; the latter complex slowly dimerizes to form the title complex. Protonation of a μ-oxo bridge is proposed to initiate the disproportionation, based on analogy with the $[Mn^{III/IV}{}_2O_2(bpy)_4]^{3+}$ system.

Introduction

The Mn tetramer of the oxygen-evolving complex (OEC) in photosystem II (PSII) is the key catalyst for the oxidation of H_2O to O_2 in plants. The recent 3.8 Å[1] and 3.7 Å[2] resolution crystal structures of PSII suggest a semiplanar/planar "Y" type structure for the Mn tetramer, though its exact nature remains unknown due to the limited resolution. Earlier XAS studies provide evidence for at least two di-μ-oxo-bridged (2.7 Å) Mn−Mn distances[3] in the OEC, while a 3.3 Å peak in the Fourier transformed EXAFS data has been assigned as backscattering from Mn.[4] Based on EXAFS results, Yachandra et al. proposed a "dimer-of-dimers" model for the OEC ("Berkeley model"),[5,6] in which two di-μ-oxo dimanganese units, each with a Mn−Mn separation of 2.7 Å, are connected via a single μ-oxo bridge to give a 3.3 Å Mn−Mn separation. The "dimer-of-dimers" model has been a leading candidate for the structure of the Mn tetramer in the OEC, although the recent X-ray structural data for PSII[1,2] and EPR/ENDOR studies[7,8] have provided support for a "3 + 1" model with a trinuclear core connected to the fourth Mn.

Despite much effort, no good synthetic analogue of the "dimer-of-dimers" model has yet been reported. Indeed, rather few high-valent Mn tetramer complexes of any sort have been synthesized.[9−11] The $[(Mn_2O_2)_2L_2]^{4+}$ complex (**1**, L = *N,N,N′,N′*-tetrakis(2-pyridyl-methyl)-2-hydroxylpropane-1,3-diamine) by Chan et al. is the closest "dimer-of-dimers" model so far.[9] We previously reported a functional system in which O_2 evolution is catalyzed by $[Mn^{III/IV}{}_2O_2(terpy)_2(H_2O)_2]^{3+}$ (**2**) upon addition of O-atom-transfer reagents such as oxone or hypochlorite.[12−14] Further studies on this system have led to the isolation of $[Mn^{IV}{}_4O_5(terpy)_4(H_2O)_2]^{6+}$ (**3**) (Figure 1). Here, we report the synthesis and properties of this complex, the first unconstrained mono-μ-oxo-bridged dimer of a pair of di-μ-oxo-bridged Mn dimers. The di-μ-oxo and mono-μ-oxo bridged Mn−Mn distances in **3** are 2.74 and 3.51 Å, respectively, which are close to the Mn−Mn distances of 2.7 and 3.3 Å obtained from the EXAFS studies of the OEC.

Experimental Section

All solutions were prepared using doubly deionized water. Compound **2**[14] and $[Mn^{IV/IV}{}_2O_2(terpy)_2(SO_4)_2]$ (**4**)[12] were synthesized following previous procedures. All other chemicals were purchased from Aldrich and used without further purification. $KHSO_5$ solutions were standardized using iodometric titrations. Elemental analyses were performed by Atlantic Microlabs Inc., Norcross, GA.

Synthesis of $[Mn^{IV}{}_4O_5(terpy)_4(H_2O)_2](ClO_4)_6$ (3). Terpy (0.147 g, 0.63 mmol) was dissolved in CH_3CN (150 mL), to which $MnCl_2\cdot10H_2O$ (0.217 g, 0.60 mmol) in H_2O (130 mL) was added. After all reactants were dissolved, the yellow mixture was stirred in an ice bath for 10 min. Oxone ($KHSO_5$, 0.323 g, 2.79 mmol/mg, 0.90 mmol) in H_2O (20 mL) was then added dropwise to the mixture, which turned deep red

(1) Zouni, A.; Witt, H. T.; Kern, J.; Fromme, P.; Krauss, N.; Saenger, W.; Orth, P. *Nature* **2001**, *409*, 739−743.
(2) Kamiya, N.; Shen, J. R. *Proc. Natl. Acad. Sci. U.S.A.* **2003**, *100*, 98−103.
(3) Kirby, J. A.; Robertson, A. S.; Smith, J. P.; Thompson, A. C.; Cooper, S. R.; Klein, M. P. *J. Am. Chem. Soc.* **1981**, *103*, 5529−5537.
(4) George, G. N.; Prince, R. C.; Cramer, S. P. *Science* **1989**, *243*, 789−791.
(5) Yachandra, V. K.; Sauer, K.; Klein, M. P. *Chem. Rev.* **1996**, *96*, 2927−2950.
(6) Yachandra, V. K.; Derose, V. J.; Latimer, M. J.; Mukerji, I.; Sauer, K.; Klein, M. P. *Science* **1993**, *260*, 675−679.
(7) Britt, R. D.; Peloquin, J. M.; Campbell, K. A. *Annu. Rev. Biophys. Biomol. Struct.* **2000**, *29*, 463−495.
(8) Peloquin, J. M.; Campbell, K. A.; Randall, D. W.; Evanchik, M. A.; Pecoraro, V. L.; Armstrong, W. H.; Britt, R. D. *J. Am. Chem. Soc.* **2000**, *122*, 10926−10942.
(9) Chan, M. K.; Armstrong, W. H. *J. Am. Chem. Soc.* **1991**, *113*, 5055−5057.
(10) Philouze, C.; Blondin, G.; Menage, S.; Auger, N.; Girerd, J. J.; Vigner, D.; Lance, M.; Nierlich, M. *Angew. Chem., Int. Ed. Engl.* **1992**, *31*, 1629−1631.
(11) Manchanda, R.; Brudvig, G. W.; Crabtree, R. H. *Coord. Chem. Rev.* **1995**, *144*, 1−38.
(12) Limburg, J.; Vrettos, J. S.; Chen, H.; de Paula, J. C.; Crabtree, R. H.; Brudvig, G. W. *J. Am. Chem. Soc.* **2001**, *123*, 423−430.
(13) Limburg, J.; Brudvig, G. W.; Crabtree, R. H. *J. Am. Chem. Soc.* **1997**, *119*, 2761−2762.
(14) Limburg, J.; Vrettos, J. S.; Liable-Sands, L. M.; Rheingold, A. L.; Crabtree, R. H.; Brudvig, G. W. *Science* **1999**, *283*, 1524−1527.

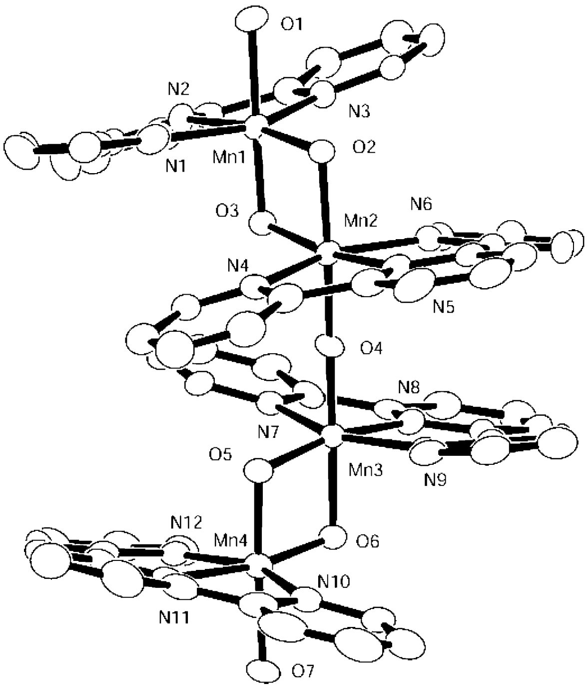

Figure 1. An ORTEP diagram of **3**, showing 30% probability thermal ellipsoids. Hydrogen atoms, perchlorate counterions, and waters of crystallization are omitted for clarity.

in about 15 min. A large excess of solid $NaClO_4$ (6.31 g) was added to the mixture, and the pH of the solution was adjusted to 2 by addition of concentrated HNO_3. (**CAUTION**: Perchlorates and their solutions are potentially explosive; even though no accident occurred during handling, extreme caution should be used.) This mixture was transferred to a series of small test tubes and allowed to slowly evaporate in the dark. Long, needlelike black-red crystals of **3**·$6H_2O$ and orange-red crystals of $Mn^{II}(terpy)_2(ClO_4)_2$ formed concomitantly in approximately 2 weeks. The needles were carefully separated and washed first with several drops of pH = 2 aq HNO_3 and then with copious amounts of diethyl ether. Drying under vacuum overnight gives the trihydrate complex (0.027 g, 9% yield based on Mn). Analysis calculated for $C_{60}H_{48}Cl_6Mn_4N_{12}O_{31}\cdot 3H_2O$: C, 37.54%; H, 2.84%; N, 8.76%. Found: C, 37.62%; H, 2.92%; N, 8.60%. IR (KBr, cm^{-1}): 3420(s, br), 3076(m, br), 1600(m), 1477(m), 1449(m), 1121(s), 1088(s, br), 1026(m), 857(w), 831(w), 775(m), 695(w), 659(w), 626(m).

Crystal Structure Determination of 3. A dark red needle crystal of **3**·$6H_2O$ having approximate dimensions 0.05 × 0.12 × 0.19 mm^3 was mounted on a fiber and immediately cooled to −90° C for data collection. Upon drying or under vacuum, water appears to be lost from the hexahydrate. All measurements were made on a Nonius KappaCCD diffractometer with graphite monochromated Mo Kα radiation. The crystallographic data are summarized in Table 1.

The structure was solved by direct methods and expanded using Fourier techniques. The non-hydrogen atoms not involved in disorders were refined anisotropically. Hydrogen atoms could not be located on the aqua ligands or on the lattice water molecules and were ignored in the refinement. Other hydrogen atoms were included in calculated positions. The lattice contained four well-defined perchlorate anions and two disordered perchlorate anions. One showed a rotational disorder, and the other was disordered over two positions. Two restraints were used to maintain the Cl−O distance. The thermal parameters of some oxygen atoms suggested partial occupancy but were refined at full occupancy. Investigation of voids using Platon[15] (with and without the disordered perchlorates and larger amplitude water oxygen atoms)

Table 1. X-ray Crystallographic Data for **3**·$6H_2O$

empirical formula	$C_{60}H_{60}Cl_6Mn_4N_{12}O_{37}$
formula weight	1973.66
crystal system	monoclinic
space group	$P2_1/c$ (#14)
a, Å	12.8890(2)
b, Å	47.3431(6)
c, Å	13.7109(2)
β, deg	113.8334(5)
V, Å^3	7653.0(2)
Z	4
T, °C	−90(1)
λ, Å	0.71069
d_{cal}, g/cm3	1.713
F_{000}	4008.00
no. of reflecns collcd/unique	20865/12775
no. observations (I > 3.00((I))	6436
reflection/parameter ratio	6.03
R^a; R_w^b	0.089; 0.097
goodness-of-fit indicator	3.94

^{a} $R = \sum||F_o| - |F_c||/\sum|F_o|$. ^{b} $R_W = [\sum w(|F_o| - |F_c|)^2/\sum wF_o^2]^{1/2}$.

indicated the presence of total uncoordinated waters in the asymmetric unit of ∼6−7. SQUEEZE[15] corrections for disordered solvent did not give satisfactory results. Multiple data collections on different crystals failed to yield a high quality data set, although all gave effectively the same structure. The mosaicity was good (0.57); however, scattering was weak and was not significant beyond 50° in 2θ. Although the metrical data should be viewed with some skepticism, the connectivity within the tetramer is secure since the uncertainties are in unimportant aspects of the structure, i.e., disordered solvent and counterions. The final cycle of full-matrix least-squares refinement on F was based on 6436 observed reflections ($I > 3.00\sigma(I)$) and 1067 variable parameters and converged with unweighted and weighted agreement factors of R = 0.089 and R_w = 0.097. Based on an occupancy of six uncoordinated water molecules per asymmetric unit, fw = 1973.66 which gives a calculated density of 1.71 g/cm^3.

EPR Spectroscopy. Perpendicular-mode EPR spectra were collected on an X-band Varian E-9 spectrometer equipped with a TE_{102} cavity and an Oxford ESR-900 liquid helium crystat. Parallel-mode EPR spectra were collected on a Bruker Biospin/ELEXSYS E500 spectrometer equipped with a TE_{012} dual mode cavity and an Oxford ESR-900 liquid helium crystat. All spectra were collected at 10 K on frozen samples with the following settings: modulation amplitude = 20 G (2 G for parallel-mode EPR spectra), modulation frequency = 100 kHz, and microwave power = 1 mW. To estimate the concentrations of **2** and Mn^{2+} in a mixture solution, scaled standard **2** and Mn^{2+} spectra were subtracted from the spectrum in question so that the residue spectrum had minimum intensity and a flat baseline. [Mn^{2+}] was estimated by the scaling factor used in the subtraction, while [**2**] was estimated by comparing the third and fourteenth peak height of a standard solution of **2** with that of the spectrum in question after subtraction of the Mn^{2+} component. In samples containing both Mn^{2+} and **2**, estimation of [Mn^{2+}] was less certain, especially at a pH close to 4.5, because the Mn^{2+} signal is completely overlapped by the 16-line signal of **2**, whereas the wings of the 16-line signal from **2** are less affected by the Mn^{2+} signal.

UV−vis Spectroscopy. UV−vis spectra were recorded on a Varian Cary-50 UV−visible spectrophotometer at room temperature using a 1 cm path length cuvette unless otherwise noted.

Electrospray Ionization Mass Spectroscopy. ESI-MS spectra were collected on a Waters/Micromass ZQ 4000 mass spectrometer. Owing to the weak signal at high mass, multiple scans over a narrow mass range were required to obtain a good signal/noise ratio. Isotope distributions were calculated using Masslynx (V4.0) and the isotope distribution calculator at http://www.sisweb.com/mstools.htm.

(15) Vandersluis, P.; Spek, A. L. *Acta Crystallogr., Sect. A* **1990**, *46*, 194−201.

Results and Discussion

Structure and Characterization of $[Mn^{IV}_4O_5(terpy)_4(H_2O)_2](ClO_4)_6$. The title compound **3** was synthesized from oxone, $MnCl_2$, and terpy in acetonitrile−water as described in the Experimental Section. The X-ray structure of **3** (Figure 1) shows the dimer-of-dimers connectivity as proposed in the Berkeley model of the OEC by Yachandra et al.[5,6] A prominent feature of **3** is that the dimers twist 90° with respect to one another. With six ClO_4^- per molecule of **3**, charge considerations require the assignment of all Mn as Mn(IV) if O(1) and O(7) are taken as H_2O, as is indeed consistent with the Mn−O distances (Mn(1)−O(1) 2.02 Å; Mn(4)−O(7) 1.99 Å). Assignment of O(1) and O(7) as OH or terminal oxo requires the assignment of Mn(V) or higher valent Mn, which are expected to be unstable within the structure in question. The Mn−Mn distances (2.74 Å) of the Mn_2O_2 cores are similar to those of known di-μ-oxo Mn dimers (2.72 Å in **2**[14] and 2.77 Å in $[Mn^{IV/IV}_2O_2(terpy)_2(SO_4)_2]$ (**4**)[12]). The higher trans-effect of the mono-μ-oxo bridge versus H_2O or SO_4^{2-} in **2** and **4**, respectively, causes the Mn(2)−O(2) and Mn(3)−O(6) distances (1.89 Å) to be longer than the di-μ-O−Mn bond lengths of **2** and **4** (1.81 and 1.83 Å, respectively). The trans-O(2)−Mn(2)−O(4) and trans-O(4)−Mn(3)−O(6) angles in **3** are 174.1° and 174.8°, with O(2)−Mn(2)−O(4)−Mn(3)−O(6) adopting a nearly linear conformation. The mono-μ-O-bridged Mn(2)−Mn(3) distance (3.51 Å) is similar to those seen in all available literature examples where a μ-oxo bridge serves as the only link between two Mn atoms (Mn−Mn distances of 3.49−3.54 Å),[16−20] with two exceptions both involving (Pc)Mn(III)−O−Mn(III)(Pc) (Pc = phthalocyanin) systems where the Mn−Mn distances are approximately 3.42 Å.[21,22] Although significantly shorter than the μ-$O_{alkoxide}$-bridged Mn−Mn distance of **1** (3.97 Å), this distance is longer than the 3.3 Å Mn−Mn separation in the OEC, which is therefore likely either to have a bent Mn−O−Mn bridge or to be connected by more than a single μ-oxo bridge.

The solid-state EPR spectrum of freshly prepared **3** (Figure 2e) consists of a very weak 16-line signal that closely resembles the solution spectrum of **2** (Figure 2a). This is consistent with an isolated mixed-valence impurity in an overall EPR-silent compound. The 16-line signal observed in solid **3** is slightly wider than that of **2** but has almost the same width as the 16-line signal in acidified aq **2** (Figure 2b, 2c) or a CH_3CN solution of **3** (spectrum not shown). No parallel-mode EPR signals were observed for powdered crystals of **3**.

Complex **3** gives an orange-red solution in both water and acetonitrile. UV−vis spectra of the two solutions (Figure 3g and 3h) show a relatively intense absorption at 471 nm (H_2O) and 481 nm (CH_3CN). ESI-MS of **3** in both solvents gives a **3** − ClO_4^- − 2 H_2O peak at m/z = 1727 and a **3** − 2 ClO_4^- − 2 H_2O + OH^- peak at m/z = 1645, with their isotopic peaks

(16) Baffert, C.; Collomb, M. N.; Deronzier, A.; Pecaut, J.; Limburg, J.; Crabtree, R. H.; Brudvig, G. W. *Inorg. Chem.* **2002**, *41*, 1404−1411.
(17) Horner, O.; Anxolabehere-Mallart, E.; Charlot, M. F.; Tchertanov, L.; Guilhem, J.; Mattioli, T. A.; Boussac, A.; Girerd, J. J. *Inorg. Chem.* **1999**, *38*, 1222−1232.
(18) Kitajima, N.; Osawa, M.; Tanaka, M.; Morooka, Y. *J. Am. Chem. Soc.* **1991**, *113*, 8952−8953.
(19) Chan, M. K.; Armstrong, W. H. *J. Am. Chem. Soc.* **1989**, *111*, 9121−9122.
(20) Schardt, B. C.; Hollander, F. J.; Hill, C. L. *J. Am. Chem. Soc.* **1982**, *104*, 3964−3972.
(21) Geiss, A.; Keller, M.; Vahrenkamp, H. *J. Organomet. Chem.* **1997**, *541*, 441−443.
(22) Vogt, L. H.; Zalkin, A.; Templeto. D. H. *Inorg. Chem.* **1967**, *6*, 1725−1730.

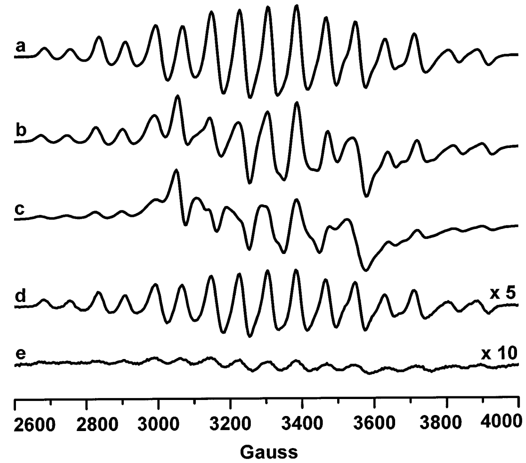

Figure 2. EPR spectra measured at 10 K of (a) 0.39 mM **2** in 0.16 M HOAc/NaOAc buffer, pH = 4.49; (b and c) same solution as that in part a, with pH adjusted to 2.50 and 2.04, respectively; (d) same solution as that in part a, with pH adjusted to 2.56 and then diluted 5 times by pH 4.5 buffer (final pH = 4.37). (e) Powdered crystals of **3** in a capillary.

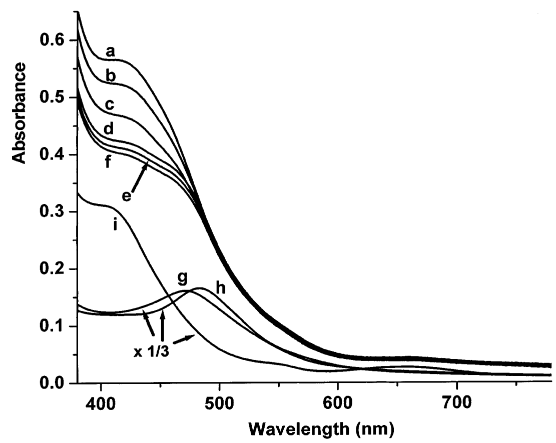

Figure 3. Formation of **3**. UV−vis spectra taken in a 0.10 cm path length cuvette. (a−f) Aliquots taken from the preparation of **3** (see Experimental Section for details) at 5, 15, 58, 390, 770, and 1440 min after adjustment of the reaction mixture to pH 2; (g) 0.62 mM **3** in H_2O; (h) 0.62 mM **3** in CH_3CN; (i) 1.2 mM **4** in H_2O.

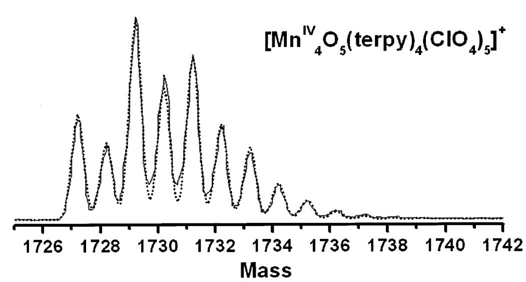

Figure 4. (Solid line) ESI-MS of **3** in CH_3CN. (Dotted line) Simulated spectrum of **3** using Gaussians generated with a line width of 0.21 mass units and with areas adjusted to the calculated isotope ratios.

closely matching the calculated isotope distribution for $[Mn^{IV}_4O_5(terpy)_4(ClO_4)_5]^+$ (Figure 4) and $[Mn^{IV}_4O_5(terpy)_4(OH)(ClO_4)_4]^+$ (not shown), respectively. The two H_2O molecules of **3** are probably lost during the desolvation process in the MS. In a CH_3CN solution of **3**, the m/z = 1645 peak is very weak but increases significantly when a small amount of H_2O (4 vol %) is added.

pH-Dependent Disproportionation of 2. Previously, we reported the synthesis of **4** from $MnSO_4$, terpy, and oxone

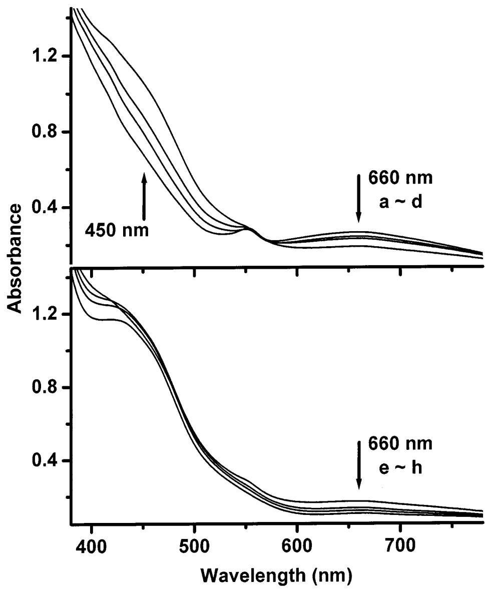

Figure 5. Biphasic UV−vis spectral change of the pH-dependent disproportionation of 0.39 mM **2** in 0.16 M HOAc/NaOAc buffer to give **4**: (a) pH = 4.49; (b) pH = 3.51; (c) pH = 3.12; (d) pH = 2.50; (e) pH = 2.38; (f) pH = 2.04; (g) pH = 1.83; (h) pH = 1.50.

(1:1:0.75) at pH = 2.[12] Compound **2** was observed to form initially and then disproportionated to give **4**, although the mechanism was not studied. In comparison, the synthesis of **3** involves $MnCl_2$, terpy, oxone (1:1.05:1.5), and excess $NaClO_4$ in CH_3CN/H_2O (pH = 2). Slow evaporation of this solution gives crystals of **3**. To better understand the solution disproprotionation chemistry of **2** leading to the formation of **3**, EPR and UV−vis studies of **2** were carried out in aqueous solution over the pH range from 1.5 to 4.5.

Upon acidification, the EPR spectrum of **2** (Figure 2a) was replaced with a 16-line signal that is slightly broader and a 6-line signal characteristic of Mn^{2+} (Figure 2b, 2c). Parallel UV−vis spectroscopy showed a biphasic spectral change. From pH = 4.49 to 2.50 (Figure 5a to 5d), the 450 nm absorption increases and the 660 nm absorption decreases with an isosbestic point at 565 nm. Further decrease of the pH caused the disappearance of **2** (550 and 660 nm) and a decrease in absorbance at 400−420 nm (Figure 5e to 5h). Both the EPR and UV−vis spectra changes were found to be partially reversible; dilution of the acidified solution by buffer (pH = 2.56 to 4.37) regenerated a clean 16-line EPR signal with no apparent Mn^{2+} component (Figure 2d). Although no precipitate was observed in this solution, the EPR signal intensity, after correction for the dilution factor, only accounts for 60−70% of total **2**. Back-titration of an acidified solution of **2** (pH = 2.5−4.5) with a concentrated NaOAc solution regenerated the original UV−vis spectra, although with smaller absorbances at 550 and 660 nm. In both cases, incubation after the addition of acid or after the subsequent dilution/addition of NaOAc up to 2 h did not improve the yield of the regenerated **2**. However, a brown solid, probably MnO_2, precipitated from the solution upon standing after NaOAc addition. Similar to what was found in the $[Mn^{III/IV}{}_2O_2(bpy)_4]^{3+}$ (bpy = 2,2′-bipyridine) system,[23,24] instability of **2** or high-valent intermediates at low pH or oligomerization (vide infra) could contribute to the incomplete reversibility in the pH titrations of **2**.

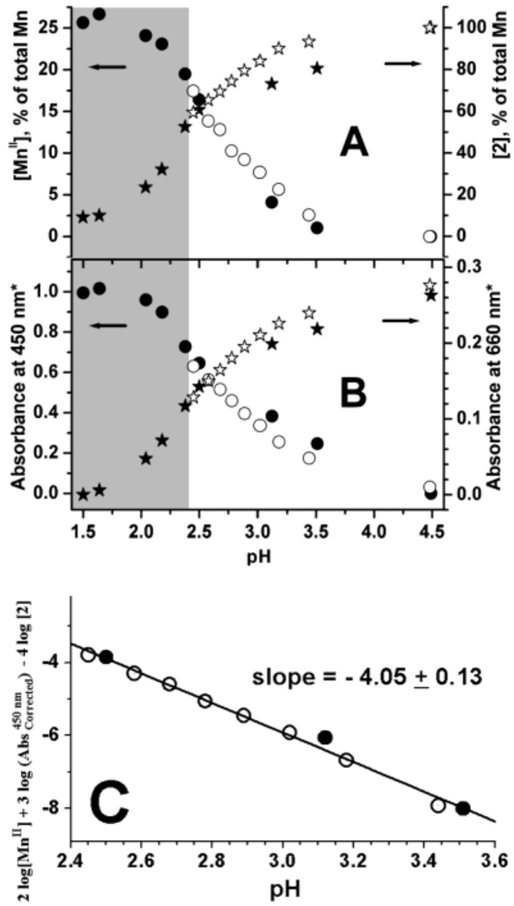

Figure 6. Correlation between the absorbance at 450 nm from Mn(IV) and 660 nm from **2**, during the pH titration of 0.39 mM **2** in 0.16 M HOAc/NaOAc buffer by concentrated HNO_3. Shading represents the pH range where nonisosbestic spectral changes were observed; solid and open symbols represent two independent sets of data. (A) EPR determination of $[Mn^{2+}]$ and [**2**] as percentage of total Mn versus pH; (B) corrected absorbance at 450 nm and 660 nm versus pH: $Abs^{450nm}{}_{corrected} = (Abs^{450nm}{}_X) - (Abs^{450nm}{}_{pH4.48}) * [\mathbf{2}]X/[\mathbf{2}]_{pH4.48}$ and $Abs^{660nm}{}_{corrected} = (Abs^{660nm}{}_X) - (Abs^{660nm}{}_{pH1.50}) * ([Mn]_{total} - 2 * [\mathbf{2}]_X)/([Mn]_{total} - 2 * [\mathbf{2}]_{pH150})$; (C) $Y = 2\log[Mn^{II}]_X + 3\log(Abs^{450nm}{}_{corrected}) - 4\log[\mathbf{2}]_X$ plot against pH. (Solid line) Linear regression fit of the data between pH = 3.6 and 2.4.

Figure 6A shows the conversion of **2** to Mn^{2+} upon pH titration as indicated by EPR spectroscopy. Given the observed stoichiometry of the disproportionation (∼0.5 Mn^{2+} per dimer), balancing of the redox states requires formation of a Mn(IV) complex, in addition to Mn^{2+}, as the major product. Since no EPR signal was observed at $g = 4$, as expected for monomeric Mn(IV) complexes such as $[Mn^{IV}(terpy)(N_3)_3]^+$,[25] the Mn(IV) complex must, therefore, be an EPR-silent oligomer like **4** or **3** (eq 1 or 2). The change in concentration of the Mn(IV) species with pH can be estimated from the absorbance change at 450 nm (after correction for the contribution of **2** at this wavelength), and the change in concentration of **2** with pH can be estimated from the absorbance change at 660 nm (after correction for the contribution of the Mn(IV) species at this wavelength). The absorbance change at the two wavelengths (Figure 6B) correlates well with the EPR signal change. Both plots give a roughly equimolar crossing point at pH ≈ 2.5.

(23) Sarneski, J. E.; Thorp, H. H.; Brudvig, G. W.; Crabtree, R. H.; Schulte, G. K. *J. Am. Chem. Soc.* **1990**, *112*, 7255−7260.
(24) Cooper, S. R.; Calvin, M. *J. Am. Chem. Soc.* **1977**, *99*, 6623−6630.
(25) Baffert, C.; Chen, H.; Crabtree, R. H.; Brudvig, G. W.; Collomb, M. N. *J. Electroanal. Chem.* **2001**, *506*, 99−105.

To test whether the disproportionation reaction could be fit to eq 1 or 2, the relative concentrations of **2**, Mn^{2+}, and the Mn(IV) complex were related to each other as a function of pH. Shown in Figure 6C is a plot of 2 log[Mn^{II}] + 3 log($Abs^{450\ nm}_{corrected}$) − 4 log[$Mn^{III/IV}{}_2$] versus pH within the pH range where isosbestic spectral changes were observed. The plot gives a straight line with a slope equal to −4.05 ± 0.13, consistent with the number of protons involved in eq 1. In contrast, a plot of 2 log[Mn^{II}] + ($^3/_2$)log($Abs^{450\ nm}_{corrected}$) − 4 log[$Mn^{III/IV}{}_2$] versus pH gives a slope equal to −3.33 ± 0.09, which does not agree with eq 2.

$$4\ [Mn^{III/IV}{}_2O_2(terpy)_2(H_2O)_2]^{3+}\ (\mathbf{2}) + 4\ H^+ \rightleftharpoons 3\ [Mn^{IV/IV}{}_2O_2(terpy)_2(H_2O)_2]^{4+}\ (\mathbf{4}) + 2\ [Mn(terpy)]^{2+} + 4\ H_2O \quad (1)$$

$$4\ [Mn^{III/IV}{}_2O_2(terpy)_2(H_2O)_2]^{3+}\ (\mathbf{2}) + H^+ \rightleftharpoons 3/2\ [Mn^{IV}{}_4O_5(terpy)_4(H_2O)_2]^{6+}\ (\mathbf{3}) + 2\ [Mn(terpy)]^{2+} + 11/2\ H_2O \quad (2)$$

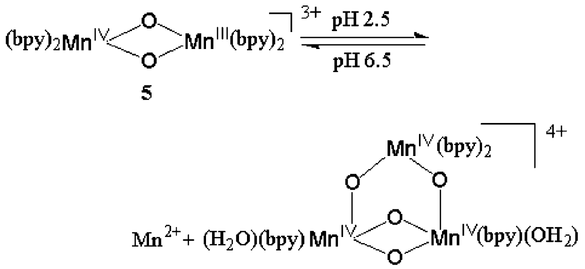

5, **6** (3)

It is reasonable to conclude, therefore, that the disproportionation reaction (2.5 < pH < 4.5) follows eq 1, since it is consistent with all of the following restrictions: (a) 0.5 Mn^{2+} per dimer is generated in the disproportionation; (b) the number of protons generated in the disproportionation is 1.0 per dimer; (c) no obvious 470 nm absorption peak from **3** was observed during the pH titration; and (d) no EPR signal other than the 16-line mixed-valence dimer signal and the 6-line Mn^{2+} signal was observed in the reaction mixture.

This disproportionation of **2** is analogous to that of $[Mn^{III/IV}{}_2O_2(bpy)_4]^{3+}$ (**5**) at low pH, where the protonation of either a μ-oxo bridge[24] or a Mn-bound bpy[26] was proposed to trigger disproportionation to Mn^{2+} and **6** (eq 3).[23] The pK_a of **5** was estimated to be 2.3 based on the pH-dependent electrochemistry results of Thorp et al.,[27] which agrees well with the solution magnetic susceptibility and optical spectroscopy data by Copper and Calvin.[24] The assignment of this pK_a to the μ-oxo bridges of **5** was supported by the comparison to the two pH-dependent redox couples of $[Mn^{III/IV}{}_2O_2(phen)_4]^{3+}$ (phen = 1,10-phenanthroline), in which case the rotation-restricted ligand rules out the possibility of stepwise protonation of the nitrogen ligand and loss of chelation.[28]

Based on these previous results for the Mn-bpy system, the crossing points of Figure 6 give a pK_a of ∼2.5 for (terpy)Mn^{III}−(μ-O)$_2$−Mn^{IV}(terpy), a value that is close to the pK_a of the Mn-bpy dimer. Protonation of the μ-oxo at low pH could destabilize **2** and favor disproportionation. The lower electron density on the μ-oxo in the resulting higher-valent Mn^{IV}−(μ-O)$_2$−Mn^{IV} is expected to shift the pK_a to a lower value. This may help stabilize the di-Mn(IV) complex at low pH. Although the meridional character of terpy prevents formation of a structure like **6**, the formation of **3** is analogous to that of **6** in the sense that extra μ-oxo bridges are formed to stabilize the high valent Mn^{IV} cluster.

Formation of 3. Compound **3** was prepared using excess oxone as oxidant, where the initially formed **2**, observed by EPR, can be regenerated from the catalyzed O_2 evolution.[12] Low pH probably helps to minimize the amount of mixed-valence impurity by promoting the disproportionation of eq 1. Dimerization of $[Mn^{IV}{}_2O_2(terpy)_2]^{4+}$, which is now the majority species in the solution, gives **3** under the condition used (eq 4). Indeed, UV−vis spectroscopy of the synthetic solution following the pH adjustment to 2 (Figure 3a−3f) shows a decrease in absorption at 400−420 nm from **4** and a new absorption growing in at 470 nm from **3**.

$$2\ [Mn^{IV/IV}{}_2O_2(terpy)_2(H_2O)_2]^{4+} \rightarrow [Mn^{IV}{}_4O_5(terpy)_4(H_2O)_2]^{6+} + H_2O + 2\ H^+ \quad (4)$$

Conclusion

We have provided evidence for the existence of the title complex **3** both in solution and in the solid state. It has the same connectivity of the μ-oxo-bridged Mn ions as in the Berkeley model proposed for the OEC.[5,6] It also has similar Mn−Mn distances as observed in the OEC. Further EXAFS and EPR studies of **3** in progress may shed light on the much-debated structure of the OEC.

Low pH was found to promote the disproportionation of $[Mn^{III/IV}{}_2O_2(terpy)_2(H_2O)_2]^{3+}$ (**2**) to Mn^{2+} and a Mn(IV)-terpy dimer, which dimerizes to form **3**. Protonation of the μ-oxo bridges may destabilize **2** and trigger the disproportionation. Although **3** has similar H_2O binding sites as **2**, previously shown to be a functional model for the OEC,[12−14] and it was isolated under conditions close to those under which O_2 evolution is seen,[12] no evidence has yet suggested that **3** plays any substantive role in the mechanism of O_2 evolution. Further studies on the mechanism of the O_2 evolution catalyzed by **2** are proceeding.

Acknowledgment. The authors thank the National Institutes of Health (GM32715) and the U.S. Department of Energy (DE-FG02-84ER13297) for financial support, K.V. Lakshmi for help with parallel-mode EPR, and Christopher Incarvito and Gerard Olack for technical assistance with ESI-MS as well as helpful discussions.

Supporting Information Available: X-ray crystallographic data of **3** (PDF); X-ray crystallographic file for **3** (CIF). This material is available free of charge via the Internet at http://pubs.acs.org.

JA037389L

(26) Manchanda, R.; Thorp, H. H.; Brudvig, G. W.; Crabtree, R. H. *Inorg. Chem.* **1992**, *31*, 4040−4041.
(27) Thorp, H. H.; Sarneski, J. E.; Brudvig, G. W.; Crabtree, R. H. *J. Am. Chem. Soc.* **1989**, *111*, 9249−9250.
(28) Manchanda, R.; Brudvig, G. W.; Crabtree, R. H. *New J. Chem.* **1994**, *18*, 561−568.